DOI:10.1158/0008-5472.CAN-06-4207

Cancer Research

Tumor-Specific Cooperation of Retinoblastoma Protein Family and Snf5 Inactivation

Jingjing Chai, Xiangdong Lu, Virginia Godfrey, et al.

Cancer Res 2007;67:3002-3009. Published online April 4, 2007.

DOI:10.1158/0008-5472.CAN-06-4207

Research Article

Tumor-Specific Cooperation of Retinoblastoma Protein Family and Snf5 Inactivation

Jingjing Chai,[1] Xiangdong Lu,[4] Virginia Godfrey,[1,4] Christopher Fletcher,[5] Charles W.M. Roberts,[6] Terry Van Dyke,[2,4] and Bernard E. Weissman[1,3,4]

Departments of [1]Pathology and Laboratory Medicine, [2]Genetics, and [3]Pediatrics and [4]UNC Lineberger Comprehensive Cancer Center, University of North Carolina, Chapel Hill, North Carolina; [5]Department of Pathology, Brigham and Women's Hospital; [6]Department of Pediatric Oncology, Dana-Farber Cancer Institute, Children's Hospital Boston and Harvard University, Boston, Massachusetts

Abstract

Malignant rhabdoid tumors (MRT) are rare aggressive cancers that occur in young children. Seventy-five percent of sporadic MRTs harbor inactivating *SNF5* mutations, and mice heterozygous for an *Snf5*-null allele develop MRTs with partial penetrance. The diagnosis of choroid plexus carcinomas (CPC) in addition to MRTs in families with a single mutant *SNF5* allele prompted us to assess the role of SNF5 loss in CPC in genetically engineered mice. With high frequency, TgT_{121} mice develop CPCs that are initiated by inactivation of retinoblastoma protein (pRb) and related proteins p107 and p130. However, CPC penetrance and latency were not significantly affected by *Snf5* heterozygosity, consistent with recent evidence that CPCs in SNF5 families were, in many cases, misdiagnosed MRTs. Surprisingly, although the CPC phenotype was unaffected, TgT_{121};$Snf5^{+/-}$ mice developed MRTs with increased penetrance and decreased latency compared with TgT_{121};$Snf5^{+/+}$ littermates. MRTs expressed the T_{121} protein with a concomitant increase in mitotic activity. The predominant appearance of TgT_{121};$Snf5^{+/-}$ MRTs in the spinal cord led to the discovery that these tumors likely arose from a subset of spinal cord neural progenitor cells expressing T_{121} rather than from transdifferentiation of CPC. Significantly, the target cell type(s) for MRT is unknown. Hence, this study not only shows that pRb_f and SNF5 inactivation cooperate to induce MRTs but also provides new insight into the MRT target population. [Cancer Res 2007;67(7):3002–9]

Introduction

Malignant rhabdoid tumors (MRT) are highly malignant pediatric renal and extrarenal tumors with unique cellular characteristics. Rhabdoid cells have large vesicular nuclei, a prominent single nucleolus, and globular eosinophilic cytoplasmic inclusions. The most frequent extrarenal site of MRTs is the central nervous system (CNS), and approximately 10% to 15% of patients with renal MRTs develop independent primary tumors of the CNS (1, 2). MRTs are extremely aggressive, with most patients perishing within 1 year after diagnosis (3, 4). Therefore, new treatment approaches for this disease remain a high priority.

Because MRTs typically consist of poorly differentiated cells with a few admixed rhabdoid cells, diagnosis based on histology alone proves difficult. However, recent studies have shown that virtually all MRTs lose expression of the *SNF5/INI1/BAF47* gene, providing a definitive diagnostic marker (5–7). The *SNF5* gene, which encodes the smallest member of the SWI/SNF chromatin remodeling complex, localizes to 22q11.2. The SNF5 protein interacts with many transcription regulators and viral proteins, such as c-MYC, p53, and HIV-IN (8–10). The SNF5 protein is highly conserved among different species with complete identity between mouse and human proteins (11).

In mice, *Snf5* deficiency results in embryonic lethality by E6.5, whereas ~15% of $Snf5^{+/-}$ mice develop rhabdoid-like tumors at 8 to 10 months of age (12–14). Conditional *Snf5* inactivation results in complete bone marrow aplasia, leading to anemia, hemorrhage, and death of most mice 1 to 3 weeks after induction (14). Furthermore, SNF5 seems essential for hepatocyte differentiation based on the phenotype of hepatocyte-specific *Snf5* deletion *in vivo* (15). These data show that *Snf5* not only is a MRT tumor suppressor but also plays a critical role in both organ and cell differentiation.

Reexpression of SNF5 in SNF5-deficient human MRT cell lines reduces phosphorylation of the retinoblastoma protein (pRb) through activation of $p16^{INK4a}$ transcription and/or inhibition of cyclin D1 expression, leading to suppression of activating E2Fs (16–20). The Rb/E2F pathway regulates cell cycle progression and plays an important role in a wide array of human cancers (21–25). A recent *in vivo* study also suggests that Rb is epistatic to SNF5 in tumor suppression (26).

Previous studies suggest that SNF5 loss might also contribute to the development of choroid plexus carcinoma (CPC; refs. 27–30), a rare pediatric tumor of the active transport epithelium located in the brain ventricles. However, because MRTs often develop in similar locations and can be difficult to diagnose based on histology alone, there is some debate as to whether MRTs and CPCs are distinct tumors both affected by SNF5 inactivation, tumor types that share a common origin, or unrelated tumors with histologic similarities that cloud diagnosis (see Discussion). Therefore, we used a genetically engineered mouse (GEM) model, TgT_{121}, in which CPCs develop with high frequency, to investigate whether loss of SNF5 contributes to CPC progression.

TgT_{121} mice express a truncated SV40 large T antigen (T_{121}) that inactivates pRb and related proteins p107 and p130 (but not p53) under the control of the lymphotropic papovavirus (LPV) promoter (31). Transgene expression is robust in the choroid plexus epithelium (CPE), predisposing to CPC, and in B and T lymphoid cells without consequence (31, 32). Dominant interference of pRb, p107, and p130 by T_{121} is an effective strategy for complete inactivation of pRb function in the mouse due to compensation of pRb inactivation by p107 and/or p130 (33–35). TgT_{121} mice develop CPCs upon spontaneous CPE p53 inactivation and become terminal ~7 months of age (36, 37).

Requests for reprints: Bernard E. Weissman, UNC Lineberger Comprehensive Cancer Center, University of North Carolina, CB#7259, Room 32-048, Chapel Hill, NC 27514. Phone: 919-966-7533; Fax: 919-966-9673; E-mail: weissman@med.unc.edu.

doi:10.1158/0008-5472.CAN-06-4207

DOI:10.1158/0008-5472.CAN-06-4207

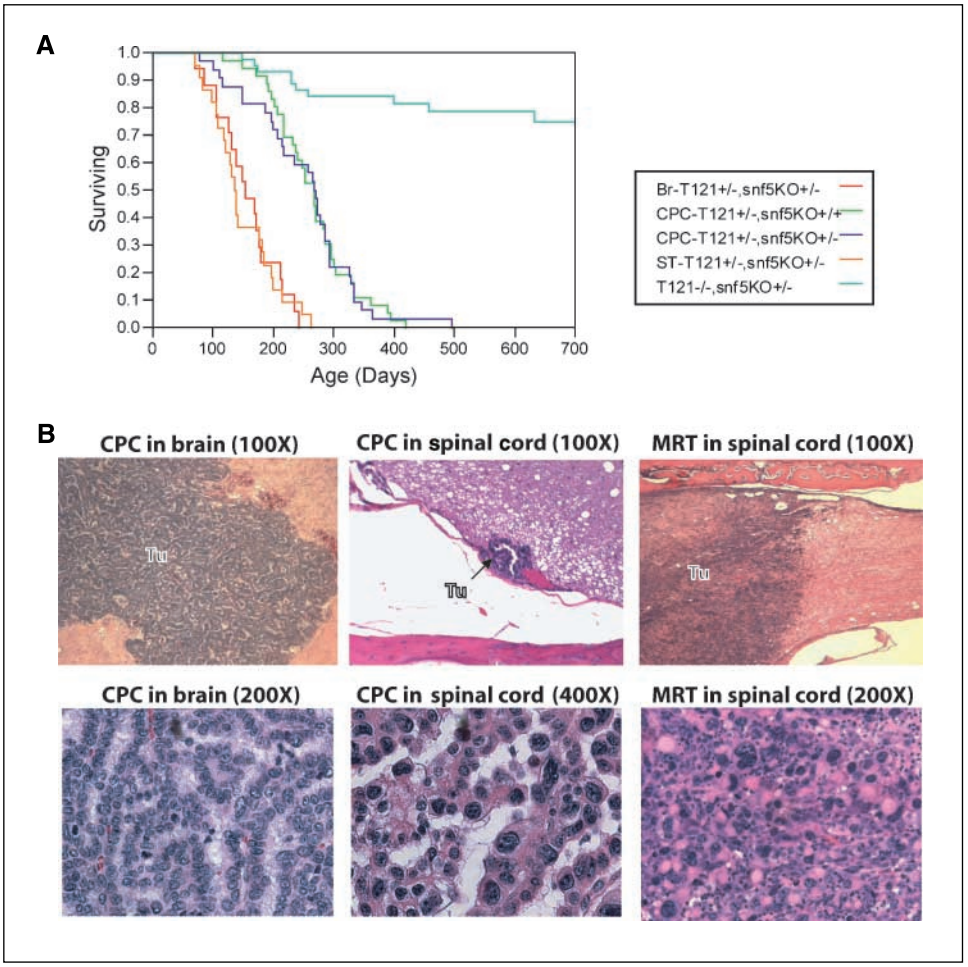

Figure 1. TgT_{121};$Snf5^{+/-}$ mice develop CPCs and MRTs in brain, soft tissues, and spinal cord. *A,* survival curves for TgT_{121}, $Snf5^{+/-}$, and TgT_{121}; $Snf5^{+/-}$ mice. *B,* H&E staining of two types of tumors at different locations in the TgT_{121};$Snf5^{+/-}$ mice. *Tu,* tumor.

Here, to examine the combined effects of pRb_f and SNF5 inactivation and to determine the relationship (if any) between CPC and MRT, we analyzed the development of these tumor types in TgT_{121};$Snf5^{+/-}$ mice. We report interesting tumor-specific differences in the cooperativity of these events. The results further provide insight into the MRT target cell type and the relationship between CPCs and MRTs.

Materials and Methods

Generation of TgT_{121};$Snf5^{+/-}$ mice. The generation, screening, and characterization of TgT_{121} transgenic (31, 36) and $Snf5^{+/-}$ (14) mice were described previously. TgT_{121};$Snf5^{+/-}$ mice were derived by crossing TgT_{121} mice with $Snf5^{+/-}$ mice. Mice with resulting genotypes, TgT_{121}, $Snf5^{+/-}$, TgT_{121};$Snf5^{+/-}$, and TgT_{121};$Snf5^{+/+}$, were born with the expected Mendelian frequencies. TgT_{121} mice were maintained on a BDF1 (The Jackson Laboratory, Bar Harbor, ME) background, and $Snf5^{+/-}$ mice were maintained on a C57BL/6 × 129/SV mixed background following procedures approved by the Institutional Animal Care and Use Committees.

Genotyping. Mice were genotyped by PCR amplification of genomic DNA from either mouse digits or postimplantation embryos (E9.5–E12.5). Mouse genomic DNA was extracted by incubating tissues with buffer A [0.2 mmol/L EDTA (pH 8.0), 25 mmol/L NaOH] at 95°C for 1 h. The lysate was neutralized by the same volume of buffer B (40 mmol/L Tris-HCl) followed by vigorous vortexing. Debris was pelleted and the supernatant was used in PCR amplification. PCR was done using the EasyStart 50 PCR kit (Molecular BioProducts, Inc., San Diego, CA). The wild-type *Snf5* allele was detected using primers against a sequence before exon 1 (Snf5-01 5′-CACCATGCCCCCACCTCCCCTACA-3′) and exon 1 (Snf5-02 5′-CAGGAAAATGGATGCAACTAAGAT-3′), whereas the *Snf5*-null allele was amplified using primers against the neo insert (in exons 1 and 2; 5′-GGCCAGCTCATTCCTCCCACTCAT-3′) and Snf5-01. T_{121}-positive animals were detected by using the primers 5′-GAATCTTTGCAGCTAATGGACC-3′ and 5′-GCATCCCAGAAGCTCCAAAG-3′. PCR conditions were as follows: 94°C for 1 min, 61°C or 59°C for 2 min, and 72°C for 1 min for 35 cycles. Agarose gel electrophoresis was used to detect the PCR products.

Genomic DNA isolation and loss of heterozygosity analysis of Snf5. Tumor genomic DNA was isolated from frozen tumor samples or from paraffin-embedded tissue slices by using the DNeasy tissue kit (Qiagen, Valencia, CA). For primary tumors, samples were crushed into a fine powder under liquid nitrogen before DNA isolation. Amplification of the *Snf5* wild-type and null alleles by PCR was done using the EasyStart 50 PCR kit using the conditions described above.

Western blot analysis. Protein concentration was quantified by the Bio-Rad protein assay (Bio-Rad Laboratories, Hercules, CA). Protein (35 μg) was separated by electrophoresis on 4% to 20% SDS-polyacrylamide gels (Cambrex, East Rutherford, NJ) and electrotransferred onto Immobilon-P membranes (Millipore, Billerica, MA) as per the manufacturers' directions. Western blot analyses of proteins were carried out by using 1:500 anti-$p16^{INK4a}$ (G175-1239; BD PharMingen, San Diego, CA), 1:1,000 anti–poly(ADP-ribose) polymerase (Roche, Indianapolis, IN), 1:1,000 anti–phosphorylated Rb (Ser^{780}; Cell Signaling, Danvers, MA), 1:1,000 anti–phosphorylated p53 (Ser^{15}; Cell Signaling), 1:1,000 anti-actin (Sigma, St. Louis, MO), and 1:2,000 horseradish peroxidase–conjugated anti-rabbit or anti-mouse IgG (Amersham, Piscataway, NJ). Individual proteins were detected with enhanced chemiluminescence reagent (Amersham) on Biomax ML film (Kodak, Rochester, NY).

DOI:10.1158/0008-5472.CAN-06-4207

Immunohistochemistry. Brain and facial tumors were fixed in 10% formalin for 16 to 20 h, whereas embryos were fixed for <1 h. Tissues were washed in running water for 3 min and saved in 70% ethanol. Bone surrounding the spinal cord was removed under a dissection microscope 3 to 4 days after fixation in 10% formalin. Sections (5 μm) were cut after embedding tissues in paraffin. For histology, sections were stained with H&E as described (31). For T_{121} and vimentin staining, sections were boiled in citrate buffer for 15 min, cooled to room temperature, and then washed twice with PBS. All sections were quenched in 3% hydrogen peroxide in methanol for 10 min at room temperature, washed in PBS thrice, and then blocked in 5% goat serum, except for T_{121} (5% horse serum), at room temperature for 30 min. Sections were incubated with an antibody to the large T antigen NH_2 terminus (1:100; Calbiochem, San Diego, CA), anti-vimentin (1:500; Biomeda, Foster City, CA), anti-S100β (1:100; DAKO, Carpinteria, CA), anti-nestin (1:100; BD PharMingen), anti-islet-1 (1:200; Developmental Studies Hybridoma Bank, Iowa City, IA), or anti-tubulin-β-III (1:200; Chemicon, Temecula, CA) at 4°C overnight. After washing in PBS thrice, the sections were incubated with anti-mouse or anti-rabbit antibody (1:333; Vector, Burlingame, CA) at room temperature for 30 min followed by washing in TS-T buffer [50 mmol/L Tris (pH 7.6), 150 mmol/L NaCl, 0.1% Tween 20] thrice. Elite avidin-biotin complex method reagent (Vector) was then added to the sections at room temperature for 30 min followed by two washes in TS-T buffer. Stains were developed in 3,3′-diaminobenzidine (DAKO) at room temperature for 2 to 10 min, rinsed in PBS, and counterstained in Light Green Counterstain (Biomeda). Sections were rinsed in H_2O and dehydrated before being mounted in Permount (Fisher Scientific, Pittsburgh, PA). Microscopy was done with a Zeiss Axioplan 2 microscope (Thornwood, NY).

Immunofluorescence. Tissues were fixed and processed as above. For immunofluorescence, sections were boiled in citrate buffer for 15 min, cooled to room temperature, and then washed twice with PBS. Sections were incubated with anti-cytokeratin (CK) 8/18 (1:450; Progen, Toowong, Queensland, Australia) at 4°C overnight, washed in PBS thrice, and incubated with Alexa Fluor 594 goat anti-guinea pig IgG (1:200; Molecular Probes, Carlsbad, CA) at room temperature in the dark for 1 h followed by three washes in PBS. The sections were sealed in 4′,6-diamidino-2-phenylindole buffer and stored at 4°C in the dark. Immunofluorescence microscopy was done using a Zeiss Axioplan 2 microscope.

Apoptosis assay. Terminal deoxynucleotidyl transferase–mediated dUTP nick end labeling staining was done following the manufacturer's instructions. In brief, formalin-fixed, paraffin-embedded tissues were deparaffinized and pretreated with proteinase K and quenched in 3% hydrogen peroxide. Strength TdT Enzyme was applied to the section for 20 min. The reaction was then stopped by stop/wash buffer for 10 min. An aliquot of anti-digoxigenin conjugate was added to the specimens, washed with PBS, and stained with peroxidase substrate. After three washes of H_2O, the slices were counterstained with Light Green Counterstain and washed in 100% *n*-butanol. Slices were then mounted with Permount after dehydration in xylene. Immunohistochemical microscopy was done under a Zeiss Axioplan 2 microscope.

Quantification of mitotic figures. Formalin-fixed, paraffin-embedded tissues were stained with H&E. At least 10 different fields of view were chosen, evenly distributed within the tumors. Total cell numbers and mitotic figures were counted using a Zeiss Axioplan 2 microscope. The percentage of cells in mitosis was calculated and graphed by GraphPad Prism 4.0 (GraphPad Software, San Diego, CA).

Histology. The tumor histopathology was evaluated independently by C.F. and V.G.

Results

***TgT_{121};$Snf5^{+/-}$* mice develop both MRTs and CPCs.** *TgT_{121};$Snf5^{+/-}$* and *TgT_{121};$Snf5^{+/+}$* cohorts were derived from matings between *TgT_{121}* and *$Snf5^{+/-}$* mice (see Materials and Methods). *TgT_{121};$Snf5^{+/+}$* and *TgT_{121};$Snf5^{+/-}$* offspring were generated at expected Mendelian ratios, indicating no deleterious effects during embryogenesis. *TgT_{121};$Snf5^{+/-}$* and *TgT_{121};$Snf5^{+/+}$* mice seemed healthy until CPCs, MRTs, or both arose. Based on histologic assessment, *TgT_{121};$Snf5^{+/+}$* mice developed exclusively CPCs, whereas *TgT_{121};$Snf5^{+/-}$* mice developed both CPCs and MRTs (Fig. 1*B*; Table 1). Thus, the tumor spectrum was unaffected by the compound genotype.

No effect of Snf5 heterozygosity on CPC tumorigenesis. All *TgT_{121};$Snf5^{+/+}$* mice developed CPC with a long latency as previously shown for *TgT_{121}* (37). The penetrance and latency were not significantly affected by the *$Snf5^{+/-}$* background, although earlier development of MRTs in many *TgT_{121};$Snf5^{+/-}$* mice precluded determination of the CPC end point in a subset of animals (Fig. 1*A*; Table 1). Nonetheless, the stage of CPC development at termination from MRTs was comparable with that of *TgT_{121}* mice of the same age (data not shown); hence, CPC penetrance was 100%. The median age of *TgT_{121};$Snf5^{+/+}$* and *TgT_{121};$Snf5^{+/-}$* mice terminal because of CPCs did not differ (9.0 months; range, 4–14 months versus 9.0 months; range, 2.5–13 months; Table 1). No statistical difference was noted based on Wilcoxon ($P > 0.67$) or log-rank ($P > 0.88$) analyses. The apparent lack of influence on CPC development by *Snf5* heterozygosity was consistent with the retention and expression of the wild-type *Snf5* allele in the CPCs from the *TgT_{121};$Snf5^{+/-}$* mice (Fig. 2).

In *TgT_{121}* mice, inactivation of pRb_f function in CPE induces both proliferation and apoptosis, with most apoptosis dependent on p53 function (36). CPE is dysplastic in all mice until ~6 weeks of age. Subsequent to this time and at variable ages, focal tumors develop that fall into two classes. Type I tumors (~40%) with classic CPC histology spontaneously loose p53 and grow aggressively, whereas type II tumors (~60%) retain p53 function, are histologically distinct, and grow slowly (37). Both subtypes arose in *TgT_{121};$Snf5^{+/-}$* mice with similar frequencies (data not shown). To determine whether *Snf5* haploinsufficiency affected CPE tumor cell proliferation in either class, mitotic indexes were calculated based on the percentage of mitotic figures. No significant difference in proliferation was detected between

Table 1. Tumor incidence in *TgT_{121};$Snf5^{+/-}$* and *TgT_{121};$Snf5^{+/+}$* mice

Genotype	Tumor/location		No. with tumors (total no.)	Median age (mo)	Penetrance (%)
TgT_{121};$Snf5^{+/-}$		CPC	32 (n = 71)	9.0	100
	MRT	Paralysis/spinal cord	17 (n = 71)	5.2	24
		Soft tissue	22 (n = 71)	4.7	31
TgT_{121};$Snf5^{+/+}$		CPC	36 (n = 36)	9.0	100
$Snf5^{+/-}$	MRT	Paralysis/spinal cord	2 (n = 45)	8	4
		Soft tissue	9 (n = 45)	10	20

DOI:10.1158/0008-5472.CAN-06-4207

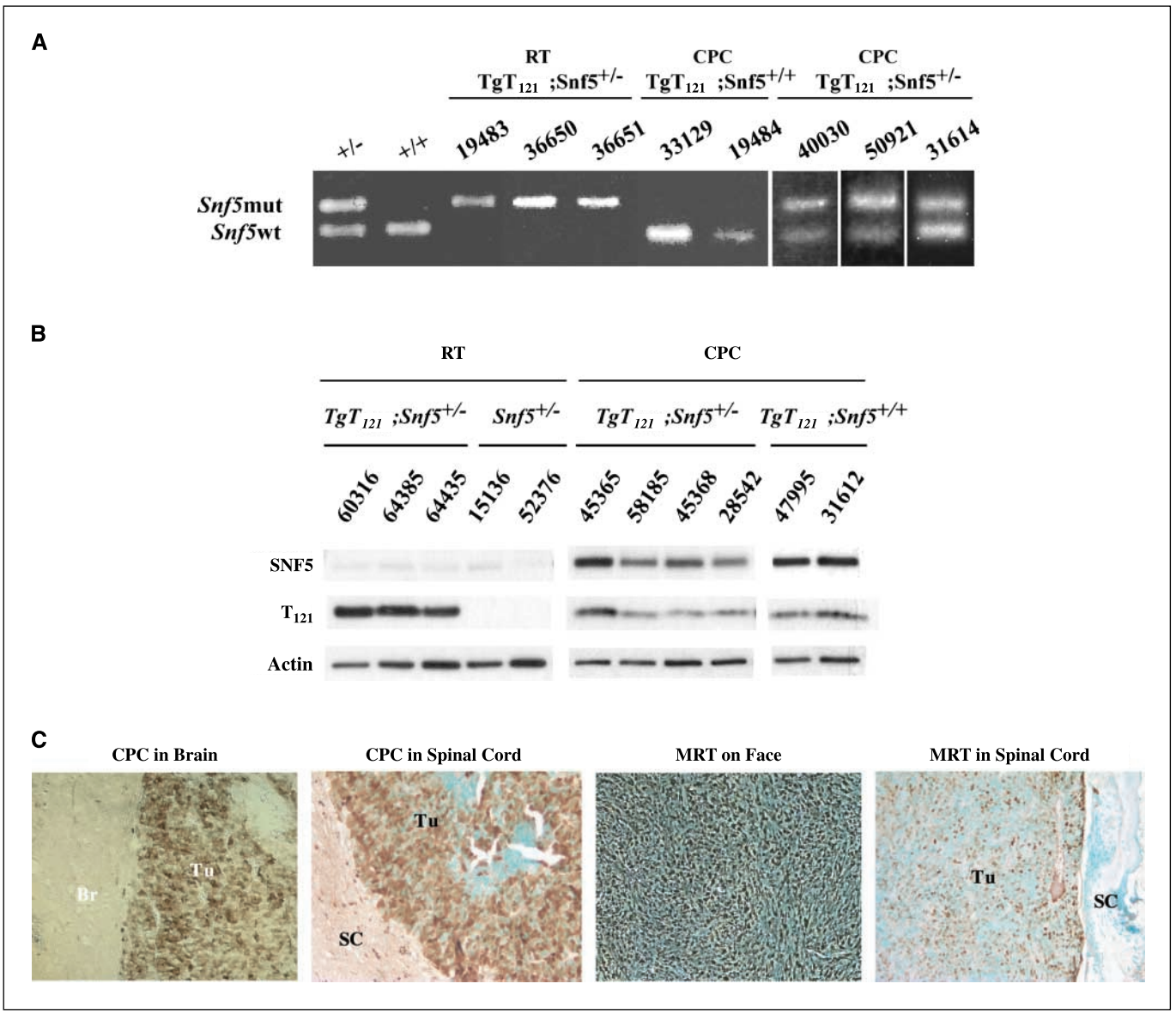

Figure 2. The wild-type Snf5 allele is selectively lost in MRT, but not in CPCs, in TgT_{121};$Snf5^{+/-}$ mice. *A,* DNA was extracted from the fresh tumor samples and amplified by PCR for both wild-type and mutant *Snf5* alleles, and the products were separated and visualized by agarose gel electrophoresis. *B,* proteins were extracted from fresh tumor samples, separated by SDS-PAGE, and immunoblotted for the indicated proteins. *C,* paraffin-embedded tumor samples from TgT_{121};$Snf5^{+/-}$ mice were characterized by immunohistochemistry for T_{121} as described in Materials and Methods. *Br,* brain; *SC,* spinal cord.

TgT_{121};$Snf5^{+/+}$ and TgT_{121};$Snf5^{+/-}$ tumors (Fig. 3). Thus, *Snf5* haploinsufficiency seems to have no detectable effect on choroid plexus tumor initiation or progression when pRb_f function is compromised. The retention of *Snf5* in terminal choroid plexus tumors also indicates no role for *Snf5* inactivation in tumor progression. These results indicate that SNF5 tumor suppression either functions through pRb_f inactivation or has no role in CPE (see Discussion).

pRb inactivation reduces latency and increases frequency of MRTs. Consistent with previous reports (12–14), only 24% of the $Snf5^{+/-}$ mice (11 of 45) became terminal with MRTs within 8 to 10 months of age at a median age of 8.2 months (range, 4–13 months; Fig. 1*A*; Table 1). These MRTs presented as soft tissue tumors mostly on the face and limbs (20%) with occasional paravertebral sites close to the distal end of spinal cord (4%). Due to the large size of the tumor, we could not determine whether the tumor originated within the spinal cord or the surrounding tissue. In combination with the T_{121} transgene, MRTs developed with increased frequency (55%) and reduced latency (median, 4.9 months; range, 2–9 months; Fig. 1*A*). Both soft tissue and CNS tumor frequencies increased (31% and 24%, respectively; Table 1). Forty-four percent (17 of 39) of the TgT_{121};$Snf5^{+/-}$ MRTs were located around the dorsal roots or spinal nerves within the spinal cord, most frequently near the thoracolumbar junction (Fig. 1*B*), with a median age of 5.2 months (range, 2.5–8.7 months). Because choroid plexus tumors develop in these mice with complete penetrance and overlapping latencies, the frequency of MRTs detected represents a minimum value.

The dramatic increase in penetrance and decrease in latency of MRTs in TgT_{121};$Snf5^{+/-}$ compared with $Snf5^{+/-}$ mice indicates

DOI:10.1158/0008-5472.CAN-06-4207

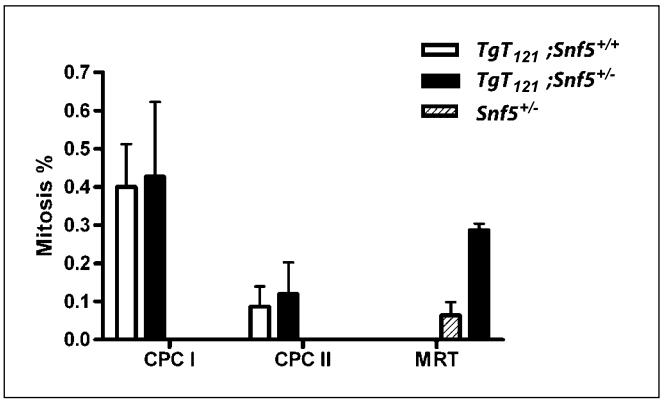

Figure 3. Mitotic rates in mouse CPC and MRT. Mitotic figures were counted in representative tumors at each time as described in Materials and Methods. *Bars,* SE.

cooperativity of pRb_f and SNF5 in MRT tumor suppression. Indeed, TgT_{121};$Snf5^{+/-}$, but not $Snf5^{+/-}$, MRTs expressed T_{121} (Fig. 2*B* and *C*). Moreover, all MRTs examined had selectively lost the wild-type *Snf5* allele (Fig. 2*A*) and failed to express SNF5 (Fig. 2*B*), further indicating that *Snf5* and pRb_f inactivation cooperate in MRT development. Significantly, TgT_{121};$Snf5^{+/-}$ MRTs (both soft tissue and CNS) had a >4-fold increased mitotic index compared with their $Snf5^{+/-}$ counterparts (Fig. 3). Increased proliferation rates could account for the increased frequency and decreased latency of TgT_{121};$Snf5^{+/-}$ MRTs. However, because the target cell population for MRTs is unknown and tumors arise in varied locations, we could not examine preneoplastic and early neoplastic proliferation rates.

Characterization of differentiation markers in MRT and CPC. Both CPC and MRT tumors have been diagnosed in SNF5 families (38), and SNF5 loss has been noted in sporadic tumors with CPC diagnosis (see Discussion). Given that only choroid plexus tumors arise in TgT_{121} mice, it was possible that *Snf5* inactivation in T_{121}-induced CPC cells facilitated conversion to MRT. Although such a hypothesis would not explain the increase in soft tissue MRTs, CPC tumors do metastasize to the spinal cord where most TgT_{121};$Snf5^{+/-}$ CNS MRTs were observed. Thus, we characterized both CPCs and MRTs for expression of differentiation markers for evidence of a CPC to MRT conversion. Human MRTs are highly positive for both vimentin and CK intermediate filaments and less commonly positive for S100β (1, 39–43). CPCs also stain positive for CK and vimentin (44, 45). A significant number of TgT_{121};$Snf5^{+/-}$ MRTs stained positive for vimentin (8 of 8) and S100β (9 of 10) by immunohistochemistry, whereas only some of the tumors were focally positive for CK8/18 (3 of 8) by immunofluorescence (Fig. 4). No difference in staining patterns was detected between soft tissue and spinal cord MRTs (Fig. 4). In contrast, all CPCs were negative for both vimentin and S100β expression, whereas the endothelium (mesenchymal origin) was positive for vimentin and the surrounding brain matter was positive for S100β (Fig. 4). Most CPCs were focally positive for CK8/18 (Fig. 4). Although CK8/18 was diffusely expressed in the cytoplasm of CPC cells, it was found in occasional agglomerates in MRT cells (Fig. 4). These findings confirm the similarity of MRTs in $Snf5^{+/-}$ mice and in human patients (46). Moreover, the distinct staining patterns of CPCs

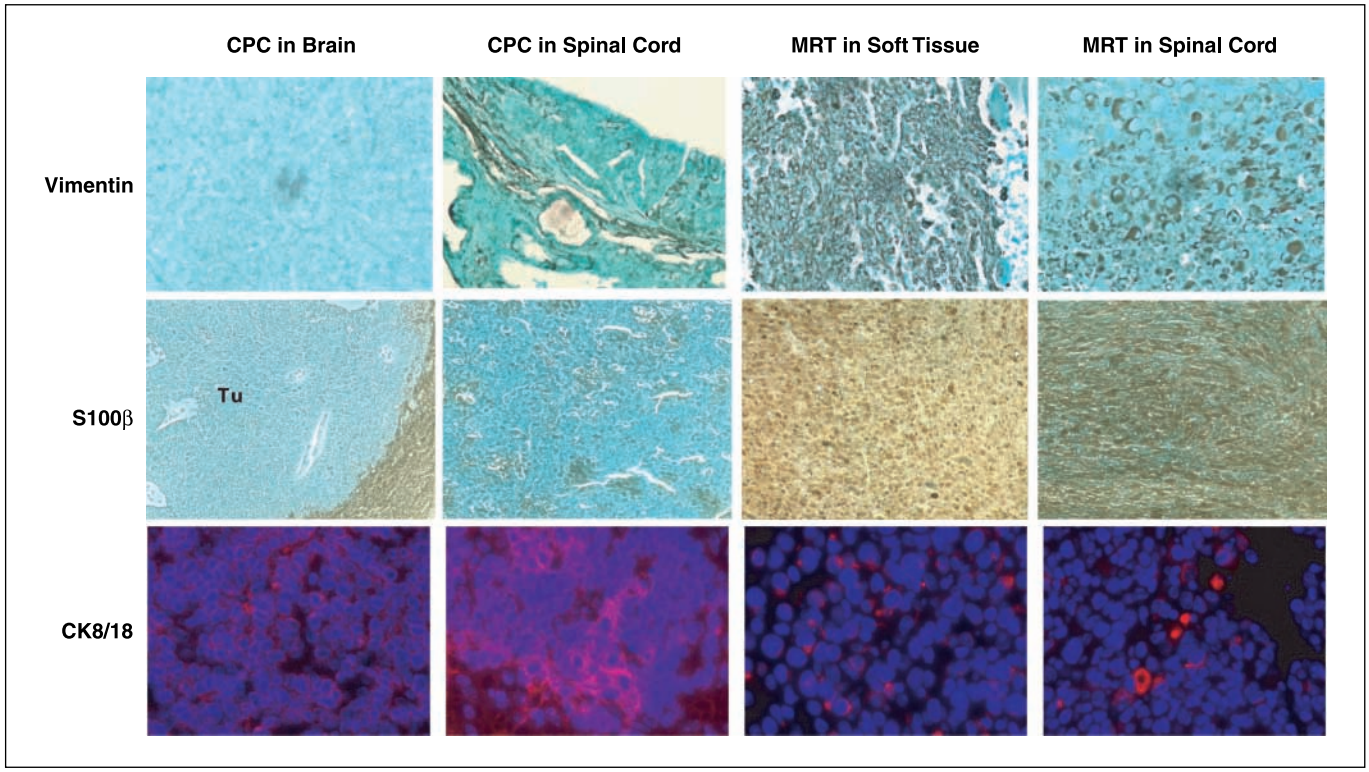

Figure 4. Differentiation marker expression in CPC and MRT. Representative CPCs and rhabdoid tumors from TgT_{121};$Snf5^{+/-}$ mice were assessed for vimentin, S100β, and CK8/18 expression by immunohistochemistry as described in Materials and Methods.

DOI:10.1158/0008-5472.CAN-06-4207

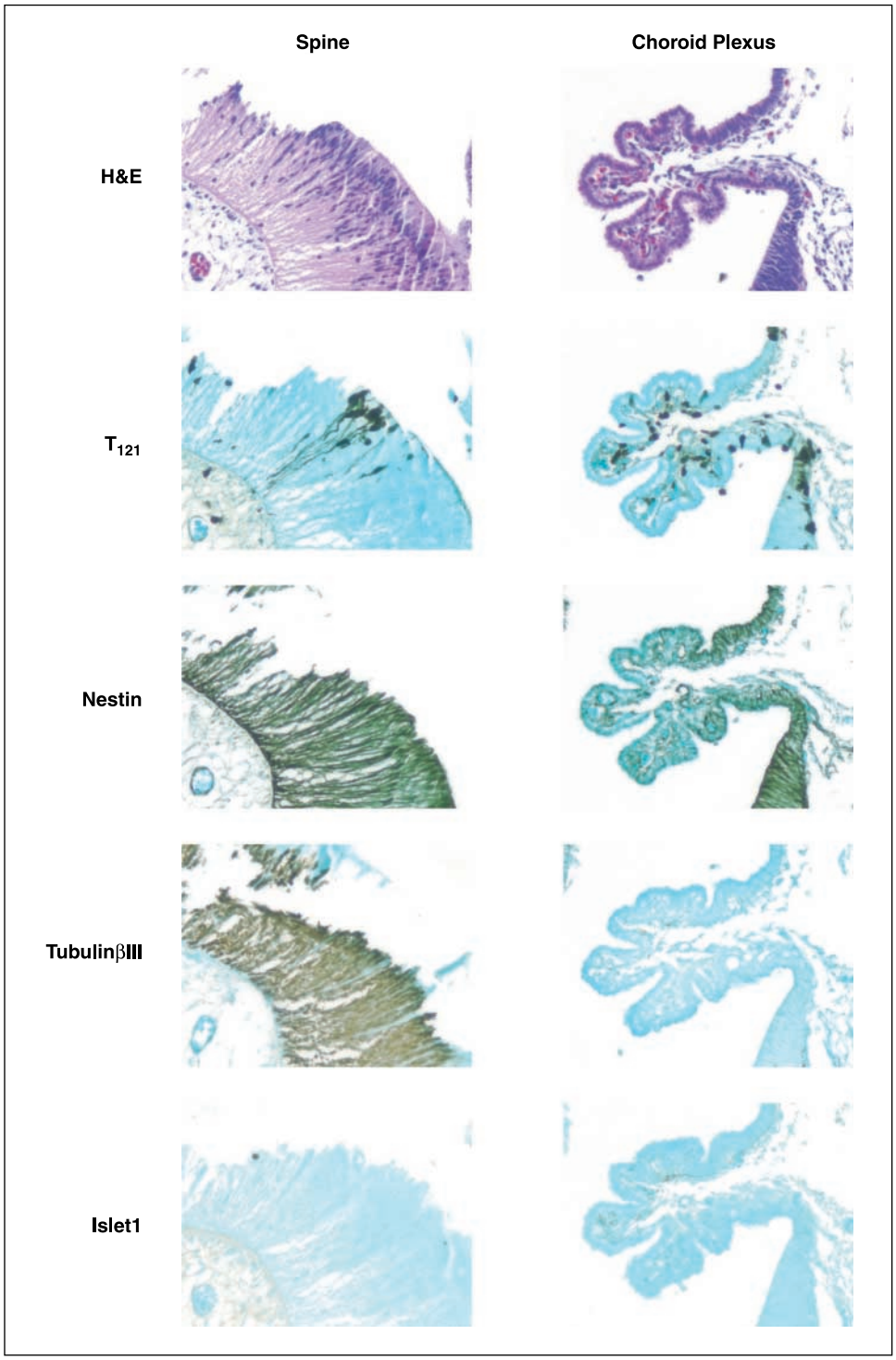

Figure 5. T_{121} expression in E12.5 mice. E12.5 embryos from *TgT_{121}* mice were fixed and stained for the indicated markers as detailed in Materials and Methods. Three different embryos were examined to confirm the expression patterns.

and MRTs within the same mice, with no evidence of conversion between types within any independent tumor analyzed, support the interpretation that these tumor types have independent and distinct origins.

T_{121} expression in non-CPE CNS cells identifies a potential MRT target population. Previous analysis of *TgT_{121}* tissues indicated that T_{121} expression is robust only in CPE and lymphoid cells. However, this study did not include spinal cord or embryonic tissues and would miss a minor subpopulation of T_{121}-expressing cells. Because the target cell population for MRTs is unknown, it is possible that T_{121} expression in previously unidentified non-CPE cells is responsible for SNF5 and pRb_f cooperativity. It is also possible that *Snf5* inactivation, which is selected for in rhabdoid tumorigenesis, ectopically induces T_{121} expression from the LPV promoter. To determine whether SNF5 loss can result in nonspecific activation of the LPV promoter, *TgT_{121};Snf5*$^{+/+}$ mouse embryo fibroblasts, which do not express the transgene, were infected with a retrovirus expressing

DOI:10.1158/0008-5472.CAN-06-4207

Snf5-specific short hairpin RNA or a dominant-negative SNF5 mutant. Despite shown reduction in SNF5 protein expression, we saw no induction of T_{121} (data not shown). Furthermore, transfection of a LPVpro-reporter vector into SNF5-deficient human MRT cell lines failed to induce luciferase activity (data not shown).

Because T_{121} expression in TgT_{121} mice may identify the MRT target cell, we analyzed TgT_{121} mouse embryos at E12.5 and E15.5 by immunohistochemistry for T_{121} expression. By E12.5, several cell types throughout the embryo were positive, including the expected CPE precursors as well as lymphoid precursors in fetal liver (Fig. 5). Importantly, a cluster of T_{121}-positive cells was located within the spinal cord near the thoracolumbar junction (the location of most TgT_{121};$Snf5^{+/-}$ CNS MRTs). These cells also expressed the neural precursor markers nestin and tubulin-β-III, but not islet-1, a neuroectoderm motor neuron progenitor marker (Fig. 5). These results raise the exciting possibility that MRTs in the TgT_{121};$Snf5^{+/-}$ mice arise from T_{121}-positive neural progenitor cells.

Discussion

MRTs are rare, poorly understood, aggressive, embryonic neoplasms. One common feature of almost all MRTs is an alteration of *SNF5* resulting in protein loss. Loss of expression mutations of *SNF5* has also been reported at a lower frequency in CPCs (29, 30, 47). Biegel et al. (48) screened 28 tumors with a submitted diagnosis of CPC by immunohistochemistry and found that seven tumors showed loss of SNF5 expression. However, reexamination of the histopathology of these tumors resulted in a revision of the diagnosis from CPC to MRT (48). Our study provides evidence to support this notion. *Snf5* haploinsufficiency did not accelerate CPC growth nor did loss of heterozygosity (LOH) of *Snf5* occur in these tumors. In contrast, MRTs in the TgT_{121};$Snf5^{+/-}$ mice selectively lost the wild-type *Snf5* allele. Thus, our findings support the conclusion from the recent human study that loss of SNF5 appears consistently in MRTs but not in CPCs (48).

The Rb family plays an important role in regulating eukaryotic cell cycle progression, apoptosis, and terminal differentiation (49). In MRTs, loss of SNF5 seems closely related to oncogenesis through the inactivation of $p16^{INK4a}$ function (17, 18, 20, 50). In addition, most primary MRTs and MRT cell lines express normal levels of an apparently wild-type Rb protein (27, 51, 52). A recent report from Guidi et al. (26) showed that $Rb^{+/-}$;$Snf5^{+/-}$ mice did not show an acceleration in tumor formation. Our results suggest that inactivation of other Rb family members, p107 and p130, accelerates MRT progression in the TgT_{121};$Snf5^{+/-}$ mice. A recent report shows the involvement of Rb, p107, and p130 in the repression of distinct sets of genes that regulate cell proliferation (53). In addition, Rb family members show different expression patterns during embryonic development (54). Therefore, it seems likely that p107 and p130 have both different and redundant functions compared with Rb in the MRT development. At present, the status of the other Rb family members in MRTs remains unknown. Further investigation will define the role of p107 and p130 in MRT development. Although we cannot exclude the possibility that pRb inactivation favors *Snf5* LOH via genetic instability, we have found no evidence for this phenomenon in our mouse models.

By immunohistochemistry, human MRTs are diffusely positive for vimentin and variably coexpress CKs and epithelial membrane antigen. Less commonly, they display focally positive staining for other markers, such as S100β, neuron-specific enolase, synaptophysin, and Leu-7 (55). The MRTs arising in the TgT_{121};$Snf5^{+/-}$ and $Snf5^{+/-}$ mice also show a similar pattern of protein expression. They were 100% positive for vimentin, a developmentally regulated intermediate filament protein found in cells of mesenchymal origin, and 90% positive for S100β, a marker widely distributed in peripheral and CNS tissues but not in epithelial cells. Thirty-eight percent of the MRTs stained positive for CK8/18, a nonsquamous epithelia marker. Interestingly, the protein appeared mainly in the classic rhabdoid cells within the cytoplasmic inclusion bodies that contain whirls of intermediate filaments. The histologic similarities between the human and mouse MRTs further validate the TgT_{121};$Snf5^{+/-}$ and $Snf5^{+/-}$ mice as appropriate models for the human disease.

Several cellular origins have been proposed for MRTs, including neuroectodermal, myogenic, histiocytic, neural, mesenchymal, and epithelial (56). Ota et al. (56) suggested that these tumors arise from primitive pluripotent cells, such as neural crest cells or the equivalent, expressing a neuroectodermal or ectomesenchymal phenotype. We found that a few neural stem cells localized at a site close to the thoracolumbar junction within the spinal cord at E12.5 expressed the T_{121} transgene, the most frequent location of the spinal MRTs in the adult mice. Considering the unexpected T_{121} expression in all MRTs, we hypothesize that the MRTs originate from a neural stem cell with an active LPV promoter. Therefore, the TgT_{121};$Snf5^{+/-}$ mice may provide the first opportunity to identify the precursor cell for MRT *in vivo* during early development. Detailed characterization of the T_{121}-positive cells with additional differentiation markers will help define the correct origin of these precursor cells. Furthermore, whereas other cell types express the T_{121} transgene at E12.5 in the TgT_{121};$Snf5^{+/-}$ mice, MRTs only appear in the same sites as the $Snf5^{+/-}$ mice (Table 1; data not shown). Therefore, our results imply that loss of SNF5 function leads to tumor development in a tissue-specific context. Further characterization of these mouse models, such as targeted disruption of *Snf5* in neural progenitor cells, will determine how SNF5 inactivation plays different roles in different cellular environments.

In summary, our results show that the loss of the Rb family increases MRT progression and occurrence within the CNS, especially the spinal cord. These findings indicate that SNF5 loss in these tumors does not equal the inactivation of all pRb function. Therefore, the TgT_{121};$Snf5^{+/-}$ mouse model provides an *in vivo* system to evaluate the interaction between inactivation of SNF5 and pRb functions to further understand the mechanism of the tumor suppressor function of SNF5. Our results also emphasize that SNF5 loss apparently drives tumor development in a tissue-dependent context. Finally, due to the high penetrance of MRTs in this GEM, the TgT_{121};$Snf5^{+/-}$ mice should prove useful for the development of new strategies for the treatment of this deadly pediatric cancer.

Acknowledgments

Received 11/14/2006; revised 1/25/2007; accepted 2/1/2007.

Grant support: PHS awards R01CA091048 (B.E. Weissman), R01CA113794 (C.W.M. Roberts), and R01CA046283 (T.V. Dyke) and The Garrett B. Smith Foundation (C.W.M. Roberts).

The costs of publication of this article were defrayed in part by the payment of page charges. This article must therefore be hereby marked *advertisement* in accordance with 18 U.S.C. Section 1734 solely to indicate this fact.

DOI:10.1158/0008-5472.CAN-06-4207

References

1. Weeks DA, Beckwith JB, Mierau GW. Rhabdoid tumor. An entity or a phenotype? Arch Pathol Lab Med 1989; 113:113–4.
2. Savla J, Chen TT, Schneider NR, Timmons CF, Delattre O, Tomlinson GE. Mutations of the hSNF5/INI1 gene in renal rhabdoid tumors with second primary brain tumors. J Natl Cancer Inst 2000;92:648–50.
3. Zimmerman MA, Goumnerova LC, Proctor M, et al. Continuous remission of newly diagnosed and relapsed central nervous system atypical teratoid/rhabdoid tumor. J Neurooncol 2005;72:77–84.
4. Tekkok IH, Sav A. Primary malignant rhabdoid tumor of the central nervous system—a comprehensive review. J Neurooncol 2005;73:241–52.
5. Biegel JA. Molecular genetics of atypical teratoid/rhabdoid tumor. Neurosurg Focus 2006;20:E11.
6. Hoot AC, Russo P, Judkins AR, Perlman EJ, Biegel JA. Immunohistochemical analysis of hSNF5/INI1 distinguishes renal and extra-renal malignant rhabdoid tumors from other pediatric soft tissue tumors. Am J Surg Pathol 2004;28:1485–91.
7. Versteege I, Sevenet N, Lange J, et al. Truncating mutations of hSNF5/INI1 in aggressive paediatric cancer. Nature 1998;394:203–6.
8. Cheng SW, Davies KP, Yung E, Beltran RJ, Yu J, Kalpana GV. c-MYC interacts with INI1/hSNF5 and requires the SWI/SNF complex for transactivation function. Nat Genet 1999;22:102–5.
9. Lee D, Sohn H, Kalpana GV, Choe J. Interaction of E1 and hSNF5 proteins stimulates replication of human papillomavirus DNA. Nature 1999;399:487–91.
10. Morozov A, Yung E, Kalpana GV. Structure-function analysis of integrase interactor 1/hSNF5L1 reveals differential properties of two repeat motifs present in the highly conserved region. Proc Natl Acad Sci U S A 1998;95:1120–5.
11. Bruder CE, Dumanski JP, Kedra D. The mouse ortholog of the human SMARCB1 gene encodes two splice forms. Biochem Biophys Res Commun 1999;257: 886–90.
12. Guidi CJ, Sands AT, Zambrowicz BP, et al. Disruption of Ini1 leads to peri-implantation lethality and tumorigenesis in mice. Mol Cell Biol 2001;21:3598–603.
13. Klochendler-Yeivin A, Fiette L, Barra J, Muchardt C, Babinet C, Yaniv M. The murine SNF5/INI1 chromatin remodeling factor is essential for embryonic development and tumor suppression. EMBO Rep 2000;1:500–6.
14. Roberts CW, Galusha SA, McMenamin ME, Fletcher CD, Orkin SH. Haploinsufficiency of Snf5 (integrase interactor 1) predisposes to malignant rhabdoid tumors in mice. Proc Natl Acad Sci U S A 2000;97: 13796–800.
15. Gresh L, Bourachot B, Reimann A, et al. The SWI/SNF chromatin-remodeling complex subunit SNF5 is essential for hepatocyte differentiation. EMBO J 2005;24: 3313–24.
16. Chai J, Charboneau AL, Betz BL, Weissman BE. Loss of the hSNF5 gene concomitantly inactivates p21CIP/WAF1 and p16INK4a activity associated with replicative senescence in A204 rhabdoid tumor cells. Cancer Res 2005;65:10192–8.
17. Betz BL, Strobeck MW, Reisman DN, Knudsen ES, Weissman BE. Re-expression of hSNF5/INI1/BAF47 in pediatric tumor cells leads to G_1 arrest associated with induction of p16ink4a and activation of RB. Oncogene 2002;21:5193–203.
18. Oruetxebarria I, Venturini F, Kekarainen T, et al. P16INK4a is required for hSNF5 chromatin remodeler-induced cellular senescence in malignant rhabdoid tumor cells. J Biol Chem 2004;279:3807–16.
19. Alarcon-Vargas D, Zhang Z, Agarwal B, Challagulla K, Mani S, Kalpana GV. Targeting cyclin D1, a downstream effector of INI1/hSNF5, in rhabdoid tumors. Oncogene 2006;25:722–34.
20. Versteege I, Medjkane S, Rouillard D, Delattre O. A key role of the hSNF5/INI1 tumour suppressor in the control of the G_1-S transition of the cell cycle. Oncogene 2002;21:6403–12.
21. Hunter T. Oncoprotein networks. Cell 1997;88: 333–46.
22. Sherr CJ. Cancer cell cycles. Science 1996;274:1672–7.
23. Weinberg RA. The retinoblastoma protein and cell cycle control. Cell 1995;81:323–30.
24. Dyson N. The regulation of E2F by pRB-family proteins. Genes Dev 1998;12:2245–62.
25. Nevins JR. The Rb/E2F pathway and cancer. Hum Mol Genet 2001;10:699–703.
26. Guidi CJ, Mudhasani R, Hoover K, et al. Functional interaction of the retinoblastoma and ini1/snf5 tumor suppressors in cell growth and pituitary tumorigenesis. Cancer Res 2006;66:8076–82.
27. DeCristofaro MF, Betz BL, Wang W, Weissman BE. Alteration of hSNF5/INI1/BAF47 detected in rhabdoid cell lines and primary rhabdomyosarcomas but not Wilms' tumors. Oncogene 1999;18:7559–65.
28. Decristofaro MF, Betz BL, Rorie CJ, Reisman DN, Wang W, Weissman BE. Characterization of SWI/SNF protein expression in human breast cancer cell lines and other malignancies. J Cell Physiol 2001;186:136–45.
29. Sevenet N, Lellouch-Tubiana A, Schofield D, et al. Spectrum of hSNF5/INI1 somatic mutations in human cancer and genotype-phenotype correlations. Hum Mol Genet 1999;8:2359–68.
30. Zakrzewska M, Wojcik I, Zakrzewski K, et al. Mutational analysis of hSNF5/INI1 and TP53 genes in choroid plexus carcinomas. Cancer Genet Cytogenet 2005;156:179–82.
31. Saenz Robles MT, Symonds H, Chen J, Van Dyke T. Induction versus progression of brain tumor development: differential functions for the pRB- and p53-targeting domains of simian virus 40 T antigen. Mol Cell Biol 1994;14:2686–98.
32. Pipas JM, Peden KW, Nathans D. Mutational analysis of simian virus 40 T antigen: isolation and characterization of mutants with deletions in the T-antigen gene. Mol Cell Biol 1983;3:203–13.
33. Lee MH, Williams BO, Mulligan G, et al. Targeted disruption of p107: functional overlap between p107 and Rb. Genes Dev 1996;10:1621–32.
34. Robanus-Maandag E, Dekker M, van der Valk M, et al. p107 is a suppressor of retinoblastoma development in pRb-deficient mice. Genes Dev 1998;12:1599–609.
35. Sage J, Mulligan GJ, Attardi LD, et al. Targeted disruption of the three Rb-related genes leads to loss of G(1) control and immortalization. Genes Dev 2000;14: 3037–50.
36. Symonds H, Krall L, Remington L, et al. p53-dependent apoptosis suppresses tumor growth and progression *in vivo*. Cell 1994;78:703–11.
37. Lu X, Magrane G, Yin C, Louis DN, Gray J, Van Dyke T. Selective inactivation of p53 facilitates mouse epithelial tumor progression without chromosomal instability. Mol Cell Biol 2001;21:6017–30.
38. Sevenet N, Sheridan E, Amram D, Schneider P, Handgretinger R, Delattre O. Constitutional mutations of the hSNF5/INI1 gene predispose to a variety of cancers. Am J Hum Genet 1999;65:1342–8.
39. Fanburg-Smith JC, Hengge M, Hengge UR, Smith JS, Jr., Miettinen M. Extrarenal rhabdoid tumors of soft tissue: a clinicopathologic and immunohistochemical study of 18 cases. Ann Diagn Pathol 1998;2: 351–62.
40. Kaiserling E, Ruck P, Handgretinger R, Leipoldt M, Hipfel R. Immunohistochemical and cytogenetic findings in malignant rhabdoid tumor. Gen Diagn Pathol 1996;141:327–37.
41. Tsokos M, Kouraklis G, Chandra RS, Bhagavan BS, Triche TJ. Malignant rhabdoid tumor of the kidney and soft tissues. Evidence for a diverse morphological and immunocytochemical phenotype. Arch Pathol Lab Med 1989;113:115–20.
42. Vogel AM, Gown AM, Caughlan J, Haas JE, Beckwith JB. Rhabdoid tumors of the kidney contain mesenchymal specific and epithelial specific intermediate filament proteins. Lab Invest 1984;50:232–8.
43. Parham DM, Shapiro DN, Downing JR, Webber BL, Douglass EC. Solid alveolar rhabdomyosarcomas with the t(2;13). Report of two cases with diagnostic implications. Am J Surg Pathol 1994;18:474–8.
44. Miettinen M, Clark R, Virtanen I. Intermediate filament proteins in choroid plexus and ependyma and their tumors. Am J Pathol 1986;123:231–40.
45. Doglioni C, Dell'Orto P, Coggi G, Iuzzolino P, Bontempini L, Viale G. Choroid plexus tumors. An immunocytochemical study with particular reference to the coexpression of intermediate filament proteins. Am J Pathol 1987;127:519–29.
46. Itakura E, Tamiya S, Morita K, et al. Subcellular distribution of cytokeratin and vimentin in malignant rhabdoid tumor: three-dimensional imaging with confocal laser scanning microscopy and double immunofluorescence. Mod Pathol 2001;14:854–61.
47. Gessi M, Giangaspero F, Pietsch T. Atypical teratoid/rhabdoid tumors and choroid plexus tumors: when genetics "surprise" pathology. Brain Pathol 2003; 13:409–14.
48. Judkins AR, Burger PC, Hamilton RL, et al. INI1 protein expression distinguishes atypical teratoid/rhabdoid tumor from choroid plexus carcinoma. J Neuropathol Exp Neurol 2005;64:391–7.
49. Simin K, Wu H, Lu L, et al. pRb inactivation in mammary cells reveals common mechanisms for tumor initiation and progression in divergent epithelia. PLoS Biol 2004;2:E22.
50. Reincke BS, Rosson GB, Oswald BW, Wright CF. INI1 expression induces cell cycle arrest and markers of senescence in malignant rhabdoid tumor cells. J Cell Physiol 2003;194:303–13.
51. Hirose M, Yamada T, Abe T, et al. Establishment and characterization of two cultured cell lines derived from malignant rhabdoid tumors of the kidney. Int J Cancer 1996;67:218–23.
52. Rosson GB, Hazen-Martin DJ, Biegel JA, et al. Establishment and molecular characterization of five cell lines derived from renal and extrarenal malignant rhabdoid tumors. Mod Pathol 1998;11:1228–37.
53. Classon M, Dyson N. p107 and p130: versatile proteins with interesting pockets. Exp Cell Res 2001; 264:135–47.
54. Spencer C, Pajovic S, Devlin H, Dinh QD, Corson TW, Gallie BL. Distinct patterns of expression of the RB gene family in mouse and human retina. Gene Expr Patterns 2005;5:687–94.
55. Peng HQ, Stanek AE, Teichberg S, Shepard B, Kahn E. Malignant rhabdoid tumor of the kidney in an adult: a case report and review of the literature. Arch Pathol Lab Med 2003;127:e371–3.
56. Ota S, Crabbe DC, Tran TN, Triche TJ, Shimada H. Malignant rhabdoid tumor. A study with two established cell lines. Cancer 1993;71:2862–72.